Mitochondrial calcium uniporter regulator 1 (MCUR1) regulates the calcium threshold for the mitochondrial permeability transition

Dipayan Chaudhuri[a,1], Daniel J. Artiga[b], Sunday A. Abiria[a], and David E. Clapham[a,c,2]

[a]Howard Hughes Medical Institute, Department of Cardiology, Boston Children's Hospital, Boston, MA 02115; [b]Harvard University, Cambridge, MA 02138; and [c]Department of Neurobiology, Harvard Medical School, Boston, MA 02115

Contributed by David E. Clapham, February 17, 2016 (sent for review February 3, 2016; reviewed by Yuriy Kirichok and Muniswamy Madesh)

During the mitochondrial permeability transition, a large channel in the inner mitochondrial membrane opens, leading to the loss of multiple mitochondrial solutes and cell death. Key triggers include excessive reactive oxygen species and mitochondrial calcium overload, factors implicated in neuronal and cardiac pathophysiology. Examining the differential behavior of mitochondrial Ca^{2+} overload in *Drosophila* versus human cells allowed us to identify a gene, *MCUR1*, which, when expressed in *Drosophila* cells, conferred permeability transition sensitive to electrophoretic Ca^{2+} uptake. Conversely, inhibiting MCUR1 in mammalian cells increased the Ca^{2+} threshold for inducing permeability transition. The effect was specific to the permeability transition induced by Ca^{2+}, and such resistance to overload translated into improved cell survival. Thus, *MCUR1* expression regulates the Ca^{2+} threshold required for permeability transition.

Drosophila | uniporter | MCU | cyclophilin D | H9C2

The mitochondrial permeability transition (MPT) pore is large, and its opening collapses the mitochondrial membrane potential ($\Delta\Psi$), depleting the matrix of solutes <1.5 kDa. The osmotic imbalance swells and disrupts mitochondria, leading to cell death. The molecular structure of the MPT pore is unknown, although cyclophilin D [peptidyl-prolyl isomerase F (PPIF)], the ADP/ATP translocase, the F1-FO-ATP synthase, and spastic paraplegia 7 are key for its function (1–5).

Key triggers for the MPT include oxidative damage and Ca^{2+} overload. Reactive oxygen species attack a cysteine residue in mammalian PPIF (6, 7), but how Ca^{2+} overload activates the pore is unknown. Elimination of the known regulators typically inhibits the sensitivity of the MPT globally, not favoring any particular trigger (8–10). Because Ca^{2+} overload promotes cell death in excitable cells, targeting this pathway selectively may prove beneficial.

To discover novel regulators specific to mitochondrial Ca^{2+} overload, we studied MPT in *Drosophila* S2R+ cells, a system where screens have identified molecules involved in Ca^{2+} transport (11–13). We found that mitochondria within these cells were resistant to Ca^{2+} overload (14) but did possess an MPT. Moreover, we identified a mammalian gene, mitochondrial calcium uniporter regulator 1 (*MCUR1*), with no known *Drosophila* homolog, which is able to alter the MPT Ca^{2+} threshold. Inhibiting this gene confers resistance from cell death mediated by mitochondrial Ca^{2+} overload.

Results

As others have described (14), mitochondria isolated from *Drosophila* S2R+ cells are frequently damaged or defective. Therefore, we measured MPT-triggered release of the 622-Da fluorescent dye, calcein, from intact mitochondria (15). To obtain a mitochondria-specific signal, calcein-loaded cells were digitonin permeabilized, releasing cytoplasmic dye and leaving only the mitochondrial calcein. Repeated pulsing with 40 μM Ca^{2+} solution produced no calcein release (Fig. 1 *A* and *B*), although mitochondria depolarized after a few pulses, consistent with prior findings (14, 16). In these prior reports, this phenomenon was interpreted as revealing that, although the *Drosophila* possessed an MPT, its pore size was too small to release most solutes and lead to swelling. However, we were able to release larger solutes (calcein) by using 50 μM phenylarsine oxide (PAO), which triggers MPT independently of Ca^{2+} (17). These experiments suggest that *Drosophila* have an MPT response, but it is resistant to Ca^{2+} overload relative to mammalian mitochondria.

The lack of Ca^{2+}-mediated MPT in *Drosophila* mitochondria could be explained by insufficient electrophoretic Ca^{2+} uptake or insensitivity to Ca^{2+}. To distinguish these possibilities, we used the Ca^{2+} ionophore ionomycin, which we found induces much higher matrix Ca^{2+} than can be achieved by electrophoretic uptake. To image intact cells, we loaded calcein for >30 min and documented that extrusion of cytoplasmic dye leaves a predominantly mitochondrial signal (Fig. S1 *A–H*). Under these conditions, ionomycin/Ca^{2+} addition produced MPT, as calcein redistributed from mitochondria to a diffusely cytoplasmic pattern (Fig. 1 *C* and *D*). We confirmed that this MPT response was Ca^{2+} dependent. First, our media included 0.5 mM EDTA to chelate trace metals that may interfere with Ca^{2+}-ionomycin transport. Second, binding the excess Ca^{2+} with EGTA abolished calcein redistribution (Fig. 1*D*). Next, we used transmission electron microscopy (EM) to examine mitochondrial morphology. Mitochondria in control cells retained normal morphology (Fig. 1*E*). Following ionomycin/Ca^{2+} treatment, cristae were disrupted and matrix contents lost, changes typical of MPT (Fig. 1*F*). Such changes were blocked by EGTA (Fig. 1*G*). To quantify the differences in mitochondria structure, we measured

Significance

Cells injured by a variety of stressors feature a form of mitochondrial dysfunction termed the permeability transition. During this process, mitochondria swell and become disrupted, ultimately leading to cell death. In excitable cells such as cardiomyocytes or neurons, such injury is often triggered by calcium overload. By screening *Drosophila* cells, we have found a protein, mitochondrial calcium uniporter regulator 1 (MCUR1), that appears to regulate the amount of calcium required to induce the permeability transition. Modulating the function of this protein acutely may prove beneficial in limiting tissue damage during diseases that feature calcium overload.

Author contributions: D.C., D.J.A., S.A.A., and D.E.C. designed research; D.C., D.J.A., and S.A.A. performed research; D.C., D.J.A., S.A.A., and D.E.C. contributed new reagents/analytic tools; D.C., D.J.A., S.A.A., and D.E.C. analyzed data; and D.C. and D.E.C. wrote the paper.

Reviewers: Y.K., University of California, San Francisco; and M.M., Temple University School of Medicine.

The authors declare no conflict of interest.

Data deposition: The human codon-optimized MCUR1 sequence reported in this paper has been deposited in the Genbank database (accession no. KT968833).

[1]Present address: Nora Eccles Harrison Cardiovascular Research and Training Institute, Department of Medicine, University of Utah, Salt Lake City, UT 84112.

[2]To whom correspondence should be addressed. Email: dclapham@enders.tch.harvard.edu.

This article contains supporting information online at www.pnas.org/lookup/suppl/doi:10.1073/pnas.1602264113/-/DCSupplemental.

www.pnas.org/cgi/doi/10.1073/pnas.1602264113

Downloaded at Palestinian Territory, occupied on December 14, 2021

www.manaraa.com

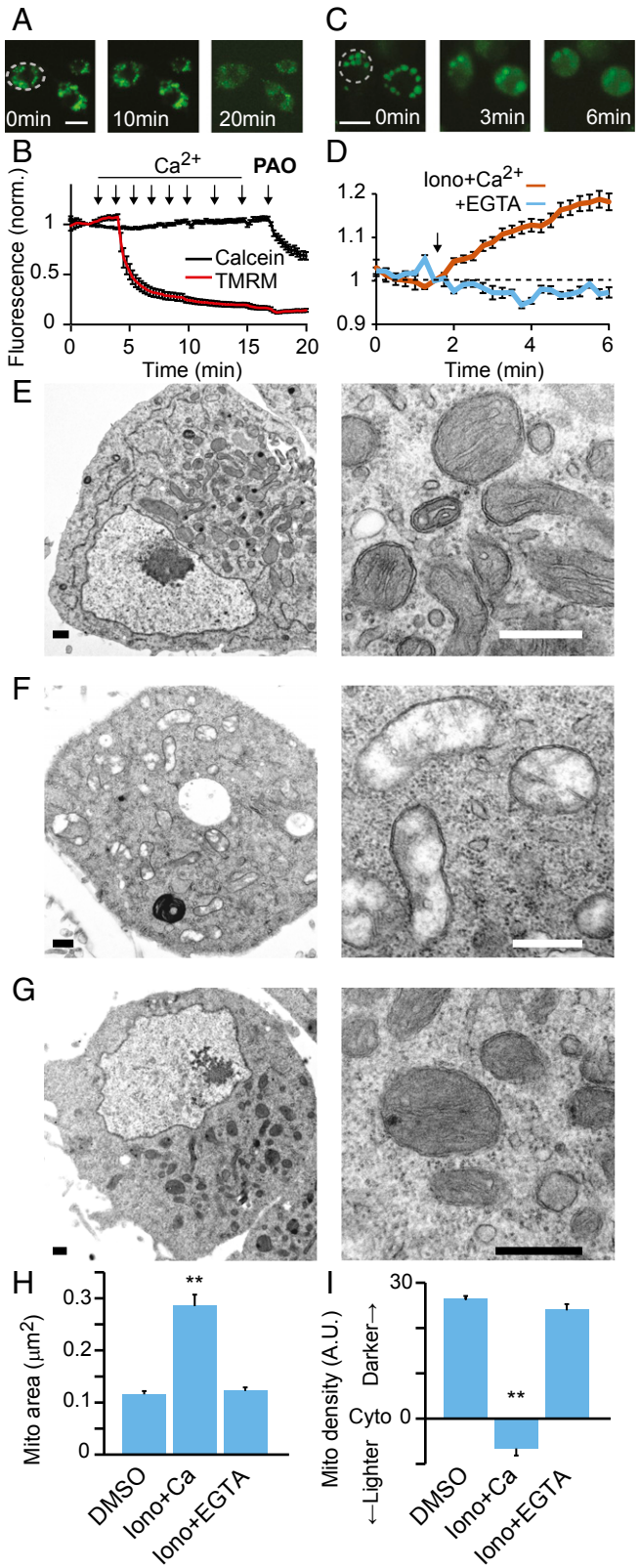

Fig. 1. *Drosophila* MPT has a high Ca^{2+} threshold. (*A* and *B*) Exemplar permeabilized *Drosophila* S2R+ cell (*A*) and summary (*B*). Mitochondria depolarize (TMRM, 50 nM) but calcein is retained during 40 μM Ca^{2+} pulses (Ca^{2+}). The 50 μM PAO releases calcein. Measurements were background subtracted and normalized to value before Ca^{2+} stimulation. Region of interest was over each whole cell, and an exemplar is shown in *A* (dashed circle). (Scale bar, 5 μm.) (n = 35 cells; error bars are SEM; and n are per condition throughout.) (*C* and *D*) Exemplar nonpermeabilized cells (*C*) and summary (*D*). Calcein exits mitochondria and redistributes throughout cells after 2 μM ionomycin/1 mM external Ca^{2+} (arrow, red trace). Redistribution abolished in 1.5 mM EGTA (green trace) ($n > 35$ cells). (*E*) Electron micrograph of S2R+ cell (*Left*), with magnified mitochondria within this cell (*Right*). Intact ultrastructure after control treatment [dimethyl sulfoxide (DMSO)]. (Scale bar, 500 nm.) (*F*) S2R+ cell treated with 2 μM ionomycin/1.5 mM Ca^{2+}. (*G*) S2R+ cell treated with EGTA and ionomycin. (*H*) Quantification of mitochondrial area from EM images ($n > 120$, $^{**}P < 0.01$). (*I*) Quantification of mitochondrial matrix density relative to surrounding cytoplasm (set to 0, $n > 120$, $^{**}P < 0.01$). Cytoplasmic densities were not statistically different across treatments.

mitochondrial area and disruption in the EM images. For disruption, we measured the average matrix density value relative to the surrounding cytoplasm, which captures the main difference between normal mitochondria (matrices darker than cytoplasm) and disrupted ones (matrices that have lost their contents, and are closer in density to/lighter than cytoplasm), and accounts for differences in exposure across images. Using these measures, we found that, after ionomycin/Ca^{2+} treatment, S2R+ mitochondria were swollen and disrupted relative to controls (Fig. 1 *H* and *I*). Thus, *Drosophila* S2R+ cells possess an MPT response but require much higher Ca^{2+} loads than can be achieved electrophoretically.

To show that Ca^{2+}-activated MPT was not exclusive to S2R+ cells (hemocyte-like, late embryonic stage derived), we tested another *Drosophila* cell line (Kc167, plasmatocyte-like, dorsal closure stage derived). These Kc167 cells also underwent MPT (Fig. S1 *I–L*), although mitochondrial disruption was not as extensive as in S2R+ cells (Fig. S1*L* versus Fig. 1*I*).

To assess whether *Drosophila* MPT employs the same mechanisms as mammalian cells, we used RNAi or pharmacological inhibition of known MPT components, PPIF and ATP/ADP translocase. PPIF is the most studied MPT regulator, and a *Drosophila* homolog (Cyp-1) has been isolated in multiple proteomic studies of purified *Drosophila* mitochondria (18, 19) (Fig. S2*A*). Fluorescently tagged Cyp-1 localized to mitochondria in S2R+ or HeLa cells; and the predicted mitochondrial-targeting sequence of Cyp-1 was sufficient to drive mCherry-tagged human PPIF into S2R+ mitochondria (Fig. S2 *B–E*). Having established that Cyp-1 localizes to mitochondria, we found that inhibiting it led to a concordant reduction in MPT, whether induced by Ca^{2+} (Fig. 2 *A* and *B*) or PAO (Fig. S2*F*). Similarly, inhibiting the known *Drosophila* ATP/ADP translocase (sesB) also reduced MPT (Fig. 2 *C* and *D*, and Fig. S2*F*).

We considered three hypotheses for the result that wild-type S2R+ MPT resisted mitochondrial Ca^{2+} overload. First, S2R+ cells may have diminished mitochondrial Ca^{2+} uptake compared with other cells (Fig. S3*A*). Second, divergence of MPT components in *Drosophila* may lead to altered function. Finally, mitochondrial proteins absent in *Drosophila* but present in mammals may confer Ca^{2+} sensitivity to MPT. To test these hypotheses, we developed S2R+ cell lines stably expressing candidate proteins. Stable lines were not clonal, as attempts to isolate individual clones led to loss of cell adherence and failure to expand. For the first hypothesis, we expressed human MCU, the pore-forming subunit of the mitochondrial Ca^{2+} uniporter that mediates the mitochondrial Ca^{2+}-selective current (20–23). For the second, we expressed human PPIF, because of the known MPT regulators, this homolog diverged most from its *Drosophila* counterpart. For the third, we identified candidates for S2R+ expression by screening for human nuclear-encoded mitochondrial genes (24) that had no homologs in the *Drosophila* genome, possessed transmembrane domains, were widely expressed, and interacted with PPIF (Fig. S3 *B* and *C*). We identified MCUR1, a potential component of the uniporter that may also function as a complex

Downloaded at Palestinian Territory, occupied on December 14, 2021

www.manaraa.com

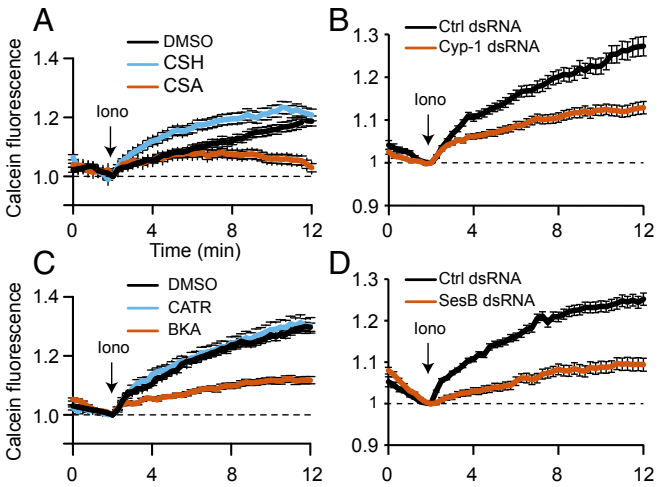

Fig. 2. S2R+ MPT is regulated by *Drosophila* homologs of PPIF and ATP/ADP translocase. (*A*) Mitochondrial calcein redistribution in intact cells stimulated with ionomycin/Ca^{2+} (arrow) as in Fig. 1*D*. Cyclosporine A (CSA) (2 μM) inhibits PPIF, whereas cyclosporine H (2 μM) does not ($n > 80$ cells per condition, $P < 0.001$). (*B*) dsRNA targeting *Drosophila* Cyp-1 inhibits Ca^{2+}-induced MPT ($n > 80$ cells per condition, $P < 0.001$). (*C*) Locking the *Drosophila* ADP/ATP translocase (*SesB*) in the *m*-conformation with 20 μM bongkrekic acid (BKA) inhibits Ca^{2+}-induced MPT, whereas the *c*-conformation stabilizer carboxyatractyloside (CATR) (2 μM) does not ($n > 50$ cells, $P < 0.001$). (*D*) dsRNA targeting *Drosophila SesB* inhibits Ca^{2+}-induced MPT ($n > 50$ cells, $P < 0.001$).

IV assembly factor (25, 26). In our S2R+ cell lines, human PPIF, MCU, and MCUR1 targeted mitochondria (Fig. 3*A*).

We first established the Ca^{2+} handling properties of the cell lines. Basal $[Ca^{2+}]_{mito}$, measured with the Ca^{2+} sensor mito-GEM-GECO (27), was greater in the MCU (2.0 ± 0.1 μM) and MCUR1 (1.1 ± 0.03 μM) lines, compared with baseline and PPIF lines (0.2 ± 0.02 μM, $n > 170$ cells for each condition). Stable S2R+ lines were more fragile than wild-type cells, and we were unable to isolate mitoplasts of suitably quality for electrophysiological assays of Ca^{2+} uptake. Instead, we monitored extramitochondrial Oregon Green BAPTA-6F fluorescence following a 10 μM Ca^{2+} pulse. Electrophoretic Ca^{2+} uptake was preserved in PPIF and MCUR1 lines but enhanced in the MCU line, as expected after increased uniporter expression (Fig. 3*B*, Fig. S3*D*, and Table S1). To test for changes in mitochondrial voltage gradients (ΔΨ), we measured the ratio of tetramethylrhodamine methyl ester (TMRM), which depends on ΔΨ, to load into mitochondria, to MitoTracker Green, which sequesters independently of ΔΨ (26), and found that MCU expression depolarizes mitochondria compared with control (Fig. 3*C*). Overexpression of either MCUR1 or PPIF did not significantly change ΔΨ relative to control.

We next queried susceptibility to Ca^{2+}-induced MPT in these lines. To produce mitochondrial Ca^{2+} overload, digitonin-permeabilized cells were incubated in media containing 200 μM Ca^{2+}, an amount sufficient to trigger mitochondrial depolarization in permeabilized cells (Fig. 1*B*). With electron micrography, we noted that only 3–14% of cells from control, MCU, or PPIF, had disrupted mitochondria, whereas in close to 30% of MCUR1 cells, Ca^{2+}-overloaded mitochondria were damaged (Fig. 3 *D* and *E*). Although this near doubling of cells with aberrant mitochondria was substantial, this measure alone understated the difference between the Ca^{2+}-treated MCUR1 line compared with the rest. For further quantitation, we focused on those cells with disrupted mitochondria. Within these cells, only 10–20% of mitochondria were altered in the control, MCU, or PPIF lines, whereas close to 60% of the mitochondria were abnormal in the MCUR1-expressing line (Fig. 3*F*), which led to obvious differences in mitochondrial area and density (Fig. 3 *G* and *H*). Of note, our S2R+ lines were nonclonal populations with variability in expression, so we speculate that particular MCUR1 clones might have had even higher fractions of cells with disrupted mitochondria.

Thus, increasing both Ca^{2+} uptake and baseline mitochondrial Ca^{2+}, via MCU expression, was insufficient to endow substantial MPT to *Drosophila* cells. Similarly, making *Drosophila* MPT components more mammalian-like, via PPIF expression, was ineffective as well. Instead, our findings suggested that MCUR1 expression makes MPT more Ca^{2+}-susceptible. We tested this hypothesis in two ways. First, we measured NADH, a mitochondria-localized fluorescent signal released during MPT (28, 29). The NADH signal located to mitochondria when measured as autofluorescence at 405-nm excitation (Fig. S3*E*) (30, 31). For mitochondrial overload, we raised intracellular Ca^{2+} levels to >1 μM with the store-operated current (32), which leads to mitochondrial Ca^{2+} uptake (13). Upon such stimulation, the NADH signal increased in the MCU line, likely from Ca^{2+}-sensitive citric acid cycle enzymes (20, 33). However, significant NADH depletion—consistent with MPT—occurred only in MCUR1 cells (Fig. S3*F*). The effect was partly reversed with cyclosporine A. Next, we determined whether this depletion resulted from mitochondrial NADH release rather than mitochondrial oxidation. After Ca^{2+} overloading mitochondria in permeabilized cells, we separated cytosolic supernatants from the mitochondria-containing pellet. Because cytoplasmic NADH oxidizes (34), we measured cytoplasmic NAD^+. Although Ca^{2+} lowered NAD^+ levels in control, PPIF, and, to a lesser extent, MCU lines, it increased NAD^+ only in MCUR1 cells (Fig. S3*G*). This would be expected if Ca^{2+}-induced MPT caused a release of mitochondrial NADH. Therefore, in several independent assays, MCUR1 expression renders S2R+ MPT susceptible to Ca^{2+} overload.

In *Drosophila*, apoptosis requires mitochondrial function but not outer membrane permeabilization and cytochrome *c* release in most cases (35, 36). This may be partly due to resistance of the inner membrane to disruption, as we found here. Thus, we examined whether inner-membrane permeabilization induced outer-membrane rupture. We Ca^{2+} overloaded permeabilized cells, separating cytoplasmic supernatants from cellular pellets, and assayed cytochrome *c* content. Although cytochrome *c* could be released by addition of the pore-forming antibiotic alamethicin (14), no other condition proved successful (Fig. S3*H*).

Having induced Ca^{2+}-mediated MPT in *Drosophila*, we turned to mammalian cells to further examine MCUR1 regulation. We acutely inhibited MCUR1 by transfecting HeLa cells with pooled siRNA (Fig. 4*A*). Compared with control, Ca^{2+} uptake, ΔΨ, and intramitochondrial pH were unaffected (Fig. 4 *B–D*, Fig. S4*A*, and Table S1), whereas basal and maximal oxygen consumption rates were reduced by such MCUR1 knockdown (Fig. 4*E*). Having established these baseline parameters of mitochondrial function, we next interrogated the Ca^{2+} sensitivity of MPT. In our first assay, we measured Ca^{2+}-induced mitochondrial depolarization, indicative of MPT, by monitoring TMRM dequenching. In this protocol, loading cells with 20 μM TMRM leads to fluorescence quenching as ΔΨ sequesters the dye in mitochondria at high concentrations. Subsequent 30 μM Ca^{2+} pulses lead to transient depolarizations and release of the dye into bulk solution, causing increases in total fluorescence, until MPT triggers complete depolarization and a significant rise in the fluorescence signal. Applying this protocol, we found that MPT was triggered earlier in control (siScr) compared with MCUR1-inhibited (siMCUR1) cells, with an almost doubling in the number of pulses required to elicit depolarization [calcium retention capacity (CRC)] (Fig. 4*F*). The effect was dependent on Ca^{2+} overload, as MCUR1 knockdown did not inhibit PAO-mediated MPT (Fig. S4*B*). Moreover, the effect was independent of the assay used. With calcein imaging, a 100 μM Ca^{2+} pulse induced release in control cells, whereas siMCUR1 cells were resistant, with some induction noted after prolonged exposure to 500 μM Ca^{2+}, despite intact PAO-mediated MPT (Fig. 4*G*). Finally, the effect was

Downloaded at Palestinian Territory, occupied on December 14, 2021
www.manaraa.com

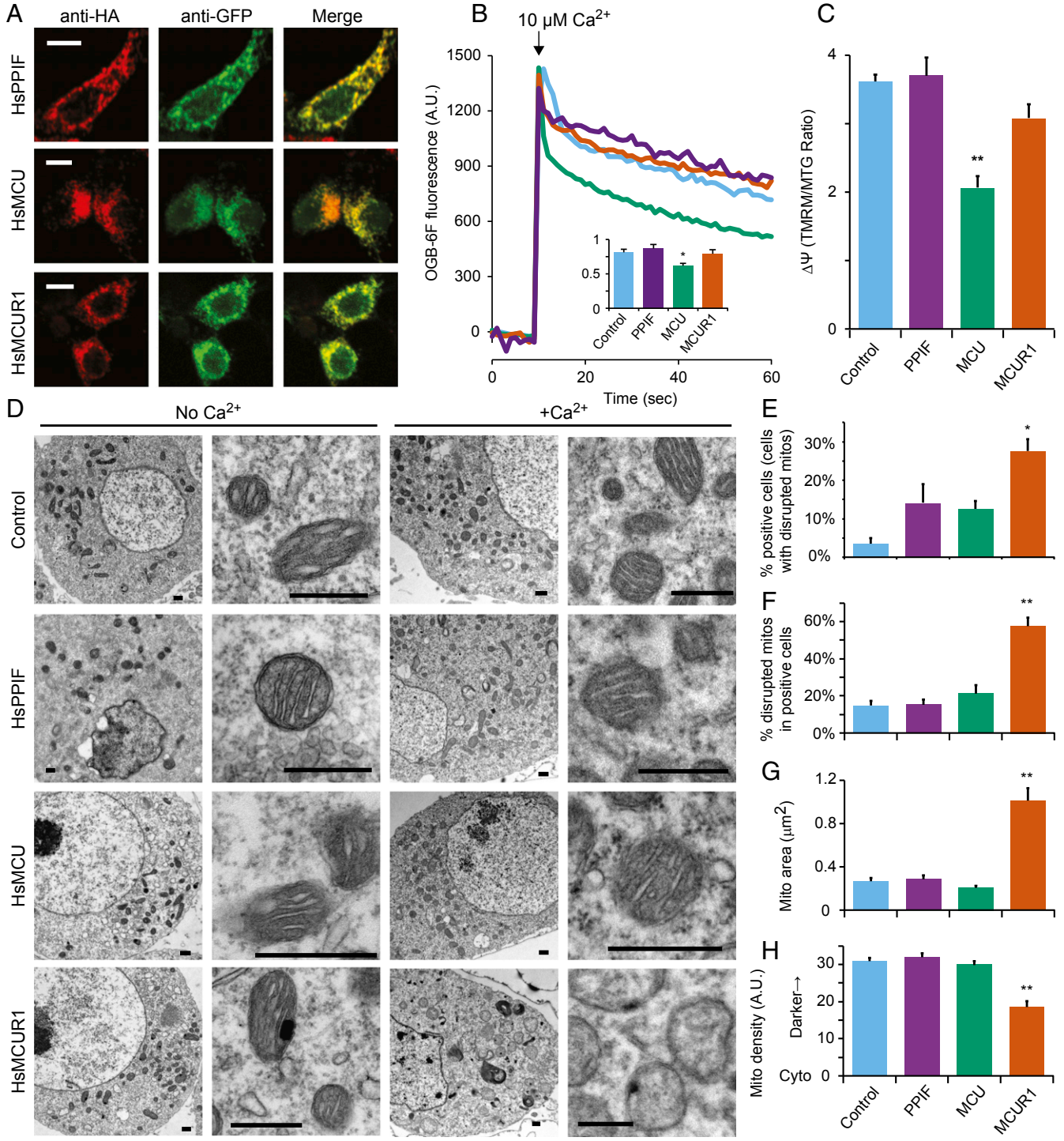

Fig. 3. MCUR1 expression lowers the Ca^{2+} threshold for MPT activation in *Drosophila* S2R+ cells. (*A*) Mitochondrial targeting of stably expressed HA-tagged human PPIF (*Top*), MCU (*Middle* row), and MCUR1 (*Bottom*). Cells cotransfected with mitochondria-targeted GFP, stained with anti-HA (*Left*) and anti-GFP (*Middle*). (*Right*) Merge. (Scale bar, 5 μm.) (*B*) Exemplar traces, 2×10^6 permeabilized S2R+ cells in a Ca^{2+}-free suspension with 1 μM Oregon Green BAPTA-6F were stimulated with 10 μM Ca^{2+} (arrow). Traces were background subtracted. (*Inset*) Fraction of peak signal noted 30 s following stimulation (n = 3–4 independent trials, $^*P < 0.05$). (*C*) Mitochondrial resting ΔΨ measured via the ratio of TMRM (50 nM, ΔΨ-dependent loading) to MitoTracker Green (100 nM, ΔΨ-independent) ($n > 120$ cells, $^{**}P < 0.01$ compared with control). (*D*) Electron micrographs of permeabilized S2R+ cells (first and third column from *Left*) and individual mitochondria within each (second and fourth column). Cells treated with vehicle (No Ca^{2+}) or 200 μM Ca^{2+} (+Ca^{2+}). Only HsMCUR1 cells display substantial amounts of damage. (Scale bar, 500 nm.) (*E*) Fraction of total cells imaged for each condition that displayed abnormal mitochondria after Ca^{2+} overload as in *D* (n = 4 reviewers, for 22–54 cells per condition, $^*P < 0.05$). (*F*) Fraction of total mitochondria that were abnormal in cells counted as having disrupted mitochondria in *E* ($n > 90$ mitochondria, for seven cells per condition, $^{**}P < 0.01$). (*G*) Mitochondrial area as in Fig. 1*H* ($n > 90$, $^{**}P < 0.01$). (*H*) Mitochondrial density as in Fig. 1*I* ($n > 90$, $^{**}P < 0.01$).

Downloaded at Palestinian Territory, occupied on December 14, 2021
www.manaraa.com

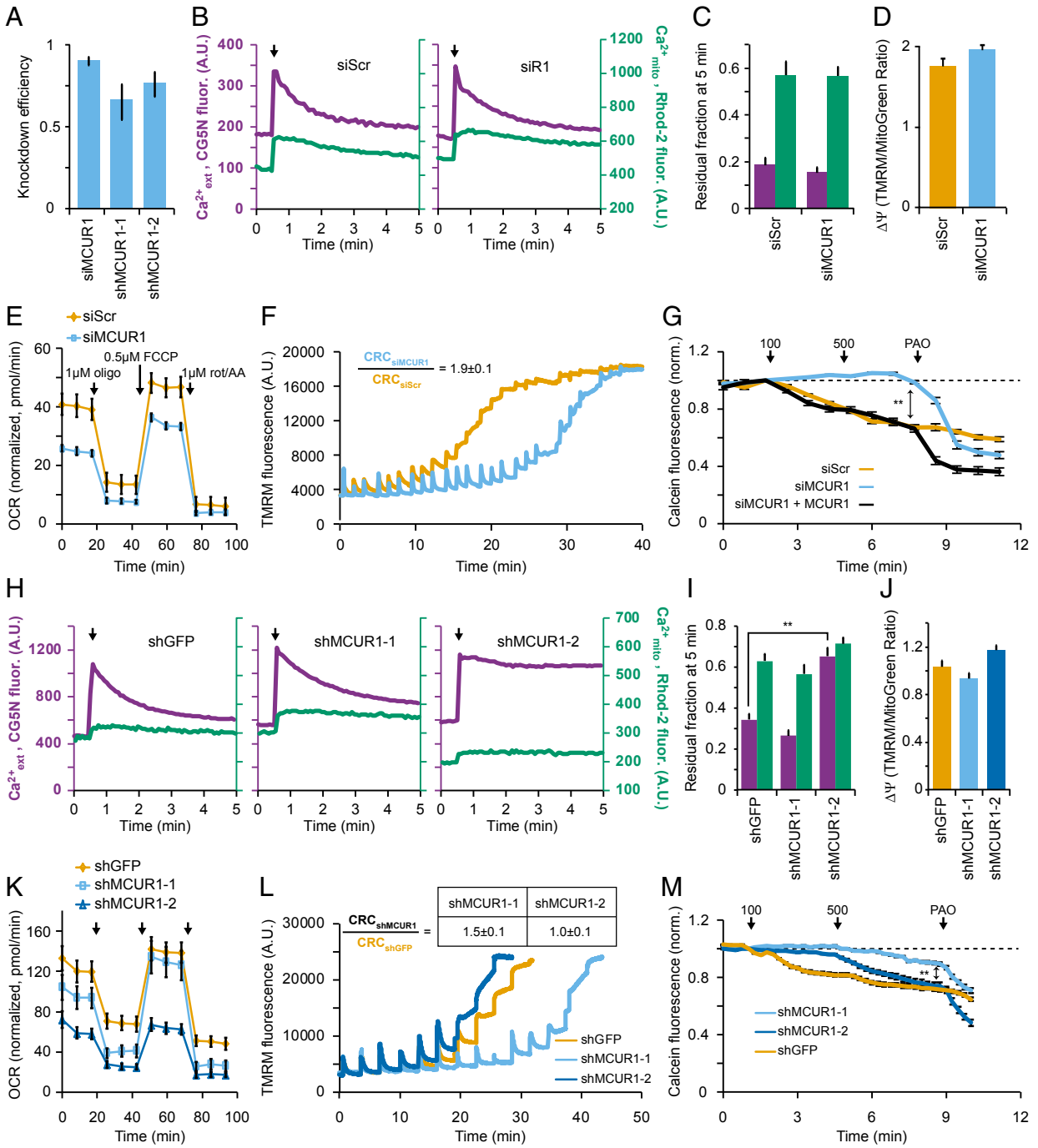

Fig. 4. MCUR1 inhibition increases the Ca^{2+} threshold for activation of the MPT. (*A*) RNAi efficacy measured using qPCR. Comparisons were between HeLa cells transfected with siRNA targeting MCUR1 (siMCUR1) and scrambled control, or between two clonal HeLa populations expressing shRNA targeting MCUR1 (shMCUR1-1 and -2) and a GFP control (shGFP). (*B*) Exemplar traces similar to Fig. 3*B*, except we used 5×10^5 cells and measured extramitochondrial Ca^{2+} ($[Ca^{2+}]_{ext}$, purple, left axis) with Calcium Green-5N and mitochondrial Ca^{2+} ($[Ca^{2+}]_{mito}$, green, right axis) with rhod-2. (*C*) Fraction of peak Ca^{2+} signal left at 5 min ($n = 4$ trials). No difference between knockdown and scrambled control (siScr) noted. (*D*) TMRM (20 nM) to MitoTracker Green (50 nM) ratio as in Fig. 3*C* ($n > 200$ cells). No difference noted between siScr and siMCUR1. (*E*) Seahorse mitochondrial stress assay. Oxygen consumption rate (OCR) measured at baseline, and after sequential additions of 1 μM oligomycin (first arrow) for ATP production, 0.5 μM FCCP (second arrow) for maximal respiration, and 1 μM rotenone/1 μM antimycin A (third arrow) for nonmitochondrial respiration. To correct for any differences in cell numbers per well, cell counts were assayed using CyQuant after protocol completion, and OCR rates were normalized to relative CyQuant fluorescence. ($n = 14$–17, $P < 0.01$). (*F*) TMRM dequenching to monitor Ca^{2+}-induced MPT. The 10^6 permeabilized HeLa cells incubated in 20 μM TMRM were stimulated every 1.5 min with 30 μM Ca^{2+}. Exemplar traces, siMCUR1- (red) and Scr-treated (blue) cells. The calcium retention capacity (CRC) is the number of additions before the mitochondria depolarize, visible as a sudden fluorescence rise ($n = 6$, $P < 0.05$). (*G*) Calcein imaging to monitor Ca^{2+}-induced MPT. Control (orange), siMCUR1 (blue), or RNA-insensitive MCUR1 (black) expressing permeabilized HeLa cells imaged during 100 μM Ca^{2+}, 500 μM Ca^{2+}, and 50 μM PAO addition (arrows) ($n = 50$–130 cells, $^{**}P < 0.001$). (*H*–*M*) Similar to *B*–*G*. (*H*) Ca^{2+} uptake blunted in the shMCUR1-2 but not shMCUR1-1 line. The baseline mitochondrial Ca^{2+} level for shMCUR1-2 was lower than the other lines ($P < 0.05$). (*I*) Fraction of peak Ca^{2+} left at 5 min ($n = 14$–16, $P < 0.01$). (*J*) No difference across groups ($n > 140$ cells). TMRM, 50 nM; MitoGreen, 100 nM. (*K*) Blunted respiration under all conditions for shMCUR1-2 ($P < 0.01$), with shMCUR1-1 showing an intermediate phenotype ($n = 12$–14). (*L*) CRC was elevated for shMCUR1-1 ($n = 15$–26, $P < 0.01$). (*M*) Calcein release was blunted for shMCUR1-1 ($n = 95$–233 cells, $^{**}P < 0.01$).

Downloaded at Palestinian Territory, occupied on December 14, 2021
www.manaraa.com

not due to siRNA off-target inhibition, as MCUR1 overexpression restored Ca^{2+} sensitivity.

A potential discrepancy between our results and those published previously (25, 26) was the absence of a Ca^{2+} uptake phenotype after MCUR1 knockdown, which we hypothesized may reflect the choice of different cell lines or the length of knockdown induced by siRNA (acute) versus shRNA (chronic). To explore this further, we produced cell lines that stably expressed an shRNA targeting MCUR1, leading to clonal lines with intermediate (~70%, shMCUR1-1) or more severe loss of MCUR1 (~80%, shMCUR1-2) compared with control (shGFP) (Fig. 4*A*). We found that the more substantial chronic loss of MCUR1 led to diminished Ca^{2+} uptake, lower baseline $[Ca^{2+}]_{mito}$, and a significant global deficit in respiration, whereas $\Delta\Psi$ remained unchanged compared with control (shMCUR1-2, Fig. 4 *H–J*, and Table S1), similar to prior results (25). Turning to the line with moderate chronic MCUR1 reduction (shMCUR1-1), we found that Ca^{2+} uptake and $\Delta\Psi$ were unchanged compared with control, and the deficit in respiration was intermediate between control and shMCUR1-2, consistent with the degree of genetic inhibition (Fig. 4 *H–K*). When we turned to assays of Ca^{2+}-stimulated MPT (Fig. 4 *L* and *M*), we were surprised to find that, whereas the cell line with moderate MCUR1 reduction (shMCUR1-1) became resistant to MPT, the cell line with more substantial reduction (shMCUR1-2) lost that resistance. This normalization of resistance may be a consequence of MCUR1's effects on cellular metabolism, as, in our hands, cell lines with more severe knockdown in MCUR1 (>85–90%) failed to expand beyond two to three splits and were unable to be tested further. Therefore, substantial acute or moderate chronic inhibition of MCUR1 leads to mitochondrial resistance to Ca^{2+} overload, whereas more substantial chronic inhibition apparently severely disrupts cellular metabolism, leading to cell death. These effects are separable, as we could maintain the MPT-resistant cells displaying moderate MCUR1 reduction (shMCUR1-1) for prolonged periods without disruption to Ca^{2+} uptake or $\Delta\Psi$.

Because our interests focused on Ca^{2+}-induced MPT, we next explored potential mechanisms for MCUR1 regulation of this threshold. For protein biochemistry, we used a codon-optimized MCUR1 transcript, as this improved plasmid expression markedly compared with the native transcript. First, we confirmed that MCUR1 interacts with PPIF and Cyp-1 (Fig. S5 *A* and *B*). We found that MCUR1 was not itself a Ca^{2+} sensor, as the MCUR1–PPIF interaction was not Ca^{2+} regulated (Fig. S5*C*), and MCUR1 inhibition increased the MPT resistance to strontium (Sr^{2+}) (Fig. S5*D*). This divalent enters mitochondria via the Ca^{2+} uniporter and disrupts $\Delta\Psi$ via MPT (23, 37). Thus, mechanistically, inhibiting MCUR1 appears to decrease the sensitivity of MPT for divalents taken up by the uniporter, independent of $\Delta\Psi$.

One potential explanation for our findings is that MCUR1 approximates the uniporter and MPT complexes, exposing the MPT Ca^{2+} sensor to higher local divalent concentrations present near the matrix face of the uniporter pore. Sensing of a local Ca^{2+} signal may partly explain why the MPT Ca^{2+} threshold is independent of matrix Ca^{2+} levels, and rather depends on total Ca^{2+} uptake (38, 39). To test this hypothesis, we assayed for interactions between MCUR1 and MCU, the pore-forming uniporter subunit (25) (Fig. S5*E*). MCUR1 bound MCU, consistent with prior reports (25, 40), but did not interact with another MPT regulator, the ATP/ADP translocase (ANT). To determine what portion of MCUR1 is critical for interactions with the uniporter and MPT channels, we generated HA-tagged constructs encoding MCUR1 segments. When cotransfected with Flag-tagged PPIF, we found that only those MCUR1 constructs containing the amino-terminal portion of the domain of unknown function 1640 (DUF1640) were able to pull down PPIF (Fig. S5*F*). Conversely, when cotransfected with Flag-tagged MCU, we found that fragments containing the MCUR1 coiled-coil domain interacted with the uniporter complex (Fig. S5*G*). When the coiled-coil domain was expressed by itself, it aggregated with MCU in a high–molecular-weight complex. Thus, the nontransmembrane portion of DUF1640 appears critical for MCUR1 protein–protein interactions.

To examine the importance of such interactions, we tested MPT in cells expressing these MCUR1 fragments. Of seven mCherry-conjugated MCUR1 fragments, six successfully targeted mitochondria. Overexpression of the DUF1640 fragment alone produced no change compared with control during MPT (fragment C, Fig. S5*H*). This fragment interacts with both the MPT and uniporter complexes, and is tethered to the inner membrane by a carboxyl-terminal transmembrane domain. By eliminating this DUF1460 transmembrane domain, we generated a construct that, when expressed, made mitochondria more susceptible to MPT (fragment E, Fig. S5*H*). Conversely, eliminating the amino-terminal portion of DUF1640 before the coiled-coil domain resulted in peptides that interacted with the uniporter but not the MPT complex (fragments D and G, Fig. S5 *G* and *H*). Remarkably, expression of these fragments led to a dominant-negative effect, inhibiting MPT (Fig. S5*H*), particularly when the construct was sequestered to the membrane (fragment D versus G). Our results suggest that MCUR1 associates with only a fraction of uniporter and MPT complexes. First, there is limited enrichment of MCU following MCUR1 immunoprecipitation, and vice versa (Fig. S5*E*). Second, expression of an MCUR1 fragment able to associate with both the uniporter and MPT channels (fragment E, Fig. S5*H*) enhanced MPT, suggesting that this peptide accesses a pool of uniporter or MPT complexes unbound by native MCUR1.

Finally, we assessed whether inhibition of MCUR1 affected cell death induced by mitochondrial Ca^{2+} overload. For these assays, we used H9c2 rat cardiomyoblasts, because investigators have defined a cell death protocol produced by mitochondrial Ca^{2+} overload (41). We assayed cellular survival by flow cytometry. First, light-scattering properties for all counted cells defined populations of live and dead/injured cells (Fig. 5*A*). Second, we stained the cells with cytoplasmic calcein (which is retained in live cells) and nuclear ethidium homodimer-1 (which stains nuclear DNA in dead cells). Their respective fluorescence levels also defined populations of cells that were live ($calcein^+$, Eth^-), dead ($calcein^-$, Eth^+), or injured ($calcein^+$, Eth^+; membranes are damaged enough to allow Eth-1 staining but not enough to completely release calcein) (Fig. 5 *B* and *C*). At baseline, cellular survival was similar after acute depletion of MCUR1 (93% inhibition via qPCR) compared with scrambled control (Fig. S6). In a first protocol, we treated cells with hydrogen peroxide (H_2O_2), as subsequent cell death is enhanced by mitochondrial Ca^{2+} (22). We found that 0.5 mM H_2O_2 induced equivalent amounts of cell survival (Fig. 5 *D* and *E*), but inhibition of MCUR1 prevented cell death, maintaining a greater fraction of cells in an injured state (Fig. 5 *E* and *F*). Next, we turned to the mitochondrial Ca^{2+} overload-specific protocol (41). Here, addition of 40 μM C2-ceramide followed by mitochondrial uptake of Ca^{2+} released from internal stores leads to substantial cell death compared with untreated cells. Remarkably, acute MCUR1 depletion improved cell survival by approximately twofold and reduced cell death by threefold (Fig. 5 *G–I*).

Discussion

Drosophila cells possess a permeability transition that is quite resistant to Ca^{2+} overload. Based on this differential phenotype, we identified a protein, MCUR1, which regulates the Ca^{2+} threshold for the MPT. When expressed in *Drosophila* S2R+ cells, MCUR1 markedly reduces the Ca^{2+} threshold for MPT. Conversely, genetic inhibition of MCUR1 made mammalian

PNAS PLUS
CELL BIOLOGY
Downloaded at Palestinian Territory, occupied on December 14, 2021
www.manaraa.com

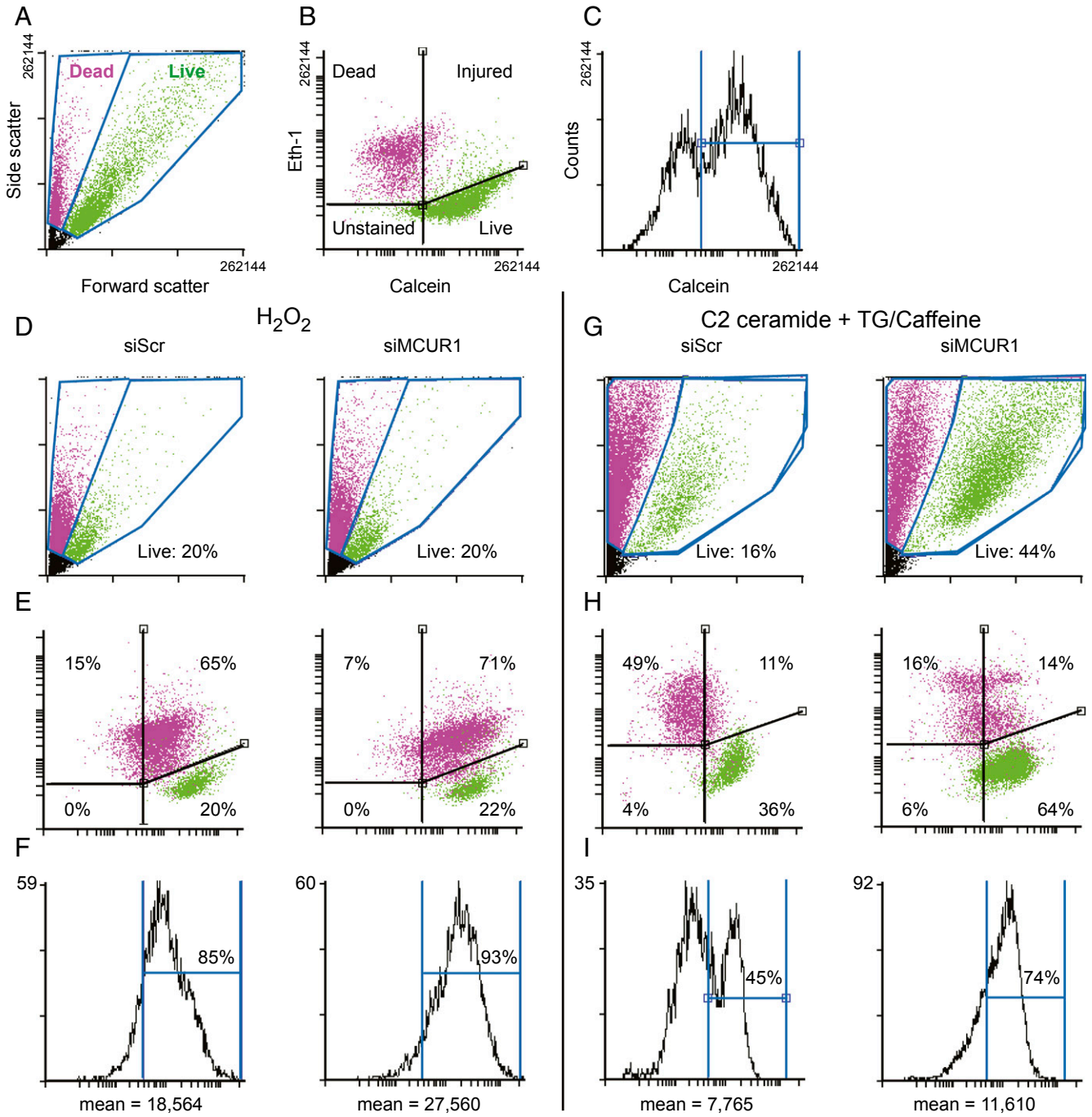

Fig. 5. *MCUR1* knockdown inhibits cell death from mitochondrial Ca^{2+} overload. (*A*) Light-scatter analysis of control, untreated cells reveals populations of live (green) and dead/injured (purple) cells. The graph displays all cells analyzed per experiment. (*B*) Live/dead analysis. Calcein and ethidium homodimer-1 (Eth-1) fluorescence levels define populations of live, injured, dead, or unstained cells. Green and purple labeling are defined in *A*. Light-scatter and fluorescence assays show good overlap for live/dead/injured classification. The graph displays a subset of cells from *A*, gated on scatter to minimize the contribution of unstained cells. (*C*) Histogram analysis of calcein levels from cells shown in *B*, with the calcein$^+$ gate (blue bars) defined as in *B*. (*D*) Analysis as in *A* for siScr or siMCUR1-treated cells after cell death induction with H_2O_2. Gating is identical for siScr and siMCUR1 throughout. Live fraction = (# of green cells) ÷ (# of green + # of purple cells). (*E*) Live/dead analysis as in *B* for H_2O_2-treated cells. (*F*) Histogram analysis of calcein levels for cells in *E*. The calcein$^+$ fraction and mean total calcein fluorescence level are displayed. (*G–I*) Analyses as in *D–F* for siScr or siMCUR1-treated cells after mitochondrial Ca^{2+} overload and cell death induced by a protocol combining C2-ceramide, thapsigargin (TG), and caffeine.

cells resistant to Ca^{2+} overload and protected them from consequent cell death.

MCUR1 was initially identified as an essential subunit of the mitochondrial Ca^{2+} uniporter (25), whereas a second report suggested that the MCUR1 helped assemble complex IV (26). The latter group suggested that MCUR1 inhibition blunts Ca^{2+} uptake by impairing OXPHOS activity and thus reducing $\Delta\Psi$. In more recent work, MCUR1 depletion blunts mitochondrial Ca^{2+} currents, even when the transmembrane voltage is clamped (42), suggesting a direct effect on the uniporter.

Downloaded at Palestinian Territory, occupied on December 14, 2021
www.manaraa.com

We did not see significant changes in ΔΨ after manipulating MCUR1 expression, consistent with the original report (25). In *Drosophila* cells, MCUR1 overexpression enhanced basal Ca^{2+} levels but did not enhance Ca^{2+} uptake rates. In mammalian cells, we did find deficits in respiration, and these appeared in a graded manner, correlated with the degree of MCUR1 depletion. The blunting of Ca^{2+} uptake follows this pattern, becoming evident after significant prolonged depletion. However, the resistance to MPT is only evident after acute or moderate MCUR1 reductions.

Our results lead to several conclusions. First, the differences between these studies may be partly due to the methodology (acute versus chronic inhibition) or cell types used. In fact, such variability in mitochondrial Ca^{2+} uptake when examining the same gene has been seen in studies focused on other components of the uniporter (43–47). Although the Ca^{2+} uptake results vary, we can conclude that MCUR1 is not essential for mitochondrial Ca^{2+} transport in all species, as *Drosophila* cells display intact Ca^{2+} uptake despite possessing no *MCUR1* homolog.

Second, MCUR1 regulation of MPT is independent of its effects on Ca^{2+} uptake rates, as (*i*) Ca^{2+} uptake does not change after MCUR1 overexpression in S2R+ cells or after acute/moderate inhibition in mammalian cells, despite altered Ca^{2+} sensitivity of the MPT, and (*ii*) enhancing the Ca^{2+} uptake rate via MCU overexpression does not induce MPT in S2R+. Such independent roles for the same protein are consistent with the behavior of other MPT components, such as the ATP/ADP translocator or the F_1-F_O-ATP synthase.

Third, MCUR1 is not the MPT Ca^{2+} sensor itself. Instead, a potential mechanism is that MCUR1 bridges the uniporter and MPT complexes, although it is not established whether these interactions involve other scaffolding proteins. This bridging hypothesis fits with prior suggestions that MCUR1 may assemble inner membrane complexes (26). Other hypotheses for MCUR1 function, such as an effect on the MPT Ca^{2+} sensor, are not excluded by this model but are difficult to investigate, because MPT Ca^{2+} sensing and matrix Ca^{2+} buffering are poorly understood.

Our results suggest that mitochondrial Ca^{2+} overload can be regulated in a MCUR1-dependent manner, and that acute manipulation of intermediates between Ca^{2+} entry and the MPT may be beneficial in treating injury due to Ca^{2+} overload.

Experimental Procedures

Detailed procedures are available in *SI Experimental Procedures*.

Mitochondrial Calcein and ΔΨ Imaging. Cells were grown for 2–3 d on coverslips. For MPT experiments, they were loaded with 1.5 μM calcein for 20–50 min, whereas for ΔΨ experiments, they were loaded for 10 min with TMRM (20–50 nM) and MitoGreen (50–100 nM). For ionomycin and ΔΨ experiments, the media was replaced with a modified Tyrode's solution before imaging. For other experiments, we permeabilized cells for 1–2 min with digitonin, and replaced media with a high-KCl solution containing 0.5 mM EGTA. Experiments were performed on an epifluorescence microscope (Olympus). For S2R+ cells, measurements were taken over the whole cell, whereas for HeLa cells, measurements were taken over the region of densest mitochondrial staining (usually perinuclear).

Calcium and TMRM Imaging. Cells were counted, washed with PBS, and incubated in a high-KCl solution containing digitonin on ice for 15 min. Cells were then spun down, washed, and resuspended in high-KCl media containing the appropriate Ca^{2+} indicator or TMRM. Aliquots were transferred to a 96-well plate, allowed to reach room temperature, and subsequently fluorescence imaged on a Flexstation 3 plate reader (Molecular Devices).

Electron Microscopy. After Ca^{2+} or control treatment, cells were fixed and imaged by modifying a protocol described previously (48).

Cell Survival Imaging. H9c2 cardiomyoblasts were treated with scrambled or MCUR1 siRNA for 3 d, and in some experiments, the procedure was repeated. Cells were treated with either 0.5 mM H_2O_2 for 6 h or 40 μM C2-ceramide, 15 mM caffeine, and 1 μM thapsigargin, as described previously (41).

Statistical Analyses. Analysis was performed using Microsoft Excel and R. We rejected the null hypothesis for $P < 0.05$. For comparisons involving $n > 15$ per condition, we used Student's *t* test. For comparisons involving $n < 15$, we used nonparametric methods, including the Kruskal–Wallis one-way ANOVA followed by Dunn's test, the Wilcoxon signed-rank test, and the Wilcoxon ranked-sum test. For assays involving multiple conditions, we compared each test condition to control using a Bonferroni correction.

ACKNOWLEDGMENTS. We thank Pichet Adstamongkonkul and Shu-Hsien Sheu for scoring electron micrographs of S2R+ cell lines, William Pu for providing H9c2 cells, Maria Ericsson for performing electron microscopy, and Quentin Gilly and Ben Housden for assistance with *Drosophila* cells. Funding was provided by American Heart Association Grant 13FTF16890003 (to D.C.), NIH Grant K99HL124070 (to D.C.), and Harvard College Research Program (D.J.A.).

1. Halestrap AP, Richardson AP (2015) The mitochondrial permeability transition: A current perspective on its identity and role in ischaemia/reperfusion injury. *J Mol Cell Cardiol* 78:129–141.
2. Giorgio V, et al. (2013) Dimers of mitochondrial ATP synthase form the permeability transition pore. *Proc Natl Acad Sci USA* 110(15):5887–5892.
3. Bonora M, et al. (2013) Role of the c subunit of the FO ATP synthase in mitochondrial permeability transition. *Cell Cycle* 12(4):674–683.
4. Alavian KN, et al. (2014) An uncoupling channel within the c-subunit ring of the F1FO ATP synthase is the mitochondrial permeability transition pore. *Proc Natl Acad Sci USA* 111(29):10580–10585.
5. Shanmughapriya S, et al. (2015) SPG7 is an essential and conserved component of the mitochondrial permeability transition pore. *Mol Cell* 60(1):47–62.
6. Linard D, et al. (2009) Redox characterization of human cyclophilin D: Identification of a new mammalian mitochondrial redox sensor? *Arch Biochem Biophys* 491(1-2): 39–45.
7. Nguyen TT, et al. (2011) Cysteine 203 of cyclophilin D is critical for cyclophilin D activation of the mitochondrial permeability transition pore. *J Biol Chem* 286(46): 40184–40192.
8. Kokoszka JE, et al. (2004) The ADP/ATP translocator is not essential for the mitochondrial permeability transition pore. *Nature* 427(6973):461–465.
9. Nakagawa T, et al. (2005) Cyclophilin D-dependent mitochondrial permeability transition regulates some necrotic but not apoptotic cell death. *Nature* 434(7033): 652–658.
10. Baines CP, et al. (2005) Loss of cyclophilin D reveals a critical role for mitochondrial permeability transition in cell death. *Nature* 434(7033):658–662.
11. Feske S, et al. (2006) A mutation in Orai1 causes immune deficiency by abrogating CRAC channel function. *Nature* 441(7090):179–185.
12. Roos J, et al. (2005) STIM1, an essential and conserved component of store-operated Ca^{2+} channel function. *J Cell Biol* 169(3):435–445.
13. Jiang D, Zhao L, Clapham DE (2009) Genome-wide RNAi screen identifies Letm1 as a mitochondrial Ca^{2+}/H^+ antiporter. *Science* 326(5949):144–147.
14. von Stockum S, et al. (2011) Properties of Ca^{2+} transport in mitochondria of *Drosophila melanogaster*. *J Biol Chem* 286(48):41163–41170.
15. Petronilli V, et al. (1999) Transient and long-lasting openings of the mitochondrial permeability transition pore can be monitored directly in intact cells by changes in mitochondrial calcein fluorescence. *Biophys J* 76(2):725–734.
16. von Stockum S, et al. (2015) F-ATPase of *Drosophila melanogaster* forms 53-picosiemen (53-pS) channels responsible for mitochondrial Ca^{2+}-induced Ca^{2+} release. *J Biol Chem* 290(8):4537–4544.
17. Lenartowicz E, Bernardi P, Azzone GF (1991) Phenylarsine oxide induces the cyclosporin A-sensitive membrane permeability transition in rat liver mitochondria. *J Bioenerg Biomembr* 23(4):679–688.
18. Lotz C, et al. (2014) Characterization, design, and function of the mitochondrial proteome: From organs to organisms. *J Proteome Res* 13(2):433–446.
19. Yin S, et al. (2013) Quantitative evaluation of the mitochondrial proteomes of *Drosophila melanogaster* adapted to extreme oxygen conditions. *PLoS One* 8(9):e74011.
20. Baughman JM, et al. (2011) Integrative genomics identifies MCU as an essential component of the mitochondrial calcium uniporter. *Nature* 476(7360):341–345.
21. Chaudhuri D, Sancak Y, Mootha VK, Clapham DE (2013) MCU encodes the pore conducting mitochondrial calcium currents. *eLife* 2:e00704.
22. De Stefani D, Raffaello A, Teardo E, Szabò I, Rizzuto R (2011) A forty-kilodalton protein of the inner membrane is the mitochondrial calcium uniporter. *Nature* 476(7360):336–340.
23. Kirichok Y, Krapivinsky G, Clapham DE (2004) The mitochondrial calcium uniporter is a highly selective ion channel. *Nature* 427(6972):360–364.
24. Pagliarini DJ, et al. (2008) A mitochondrial protein compendium elucidates complex I disease biology. *Cell* 134(1):112–123.
25. Mallilankaraman K, et al. (2012) MCUR1 is an essential component of mitochondrial Ca^{2+} uptake that regulates cellular metabolism. *Nat Cell Biol* 14(12):1336–1343.
26. Paupe V, Prudent J, Dassa EP, Rendon OZ, Shoubridge EA (2015) CCDC90A (MCUR1) is a cytochrome c oxidase assembly factor and not a regulator of the mitochondrial calcium uniporter. *Cell Metab* 21(1):109–116.

Downloaded at Palestinian Territory, occupied on December 14, 2021

www.manaraa.com

27. Zhao Y, et al. (2011) An expanded palette of genetically encoded Ca^{2+} indicators. *Science* 333(6051):1888–1891.
28. Di Lisa F, Menabò R, Canton M, Barile M, Bernardi P (2001) Opening of the mitochondrial permeability transition pore causes depletion of mitochondrial and cytosolic NAD+ and is a causative event in the death of myocytes in postischemic reperfusion of the heart. *J Biol Chem* 276(4):2571–2575.
29. Dumas JF, et al. (2009) Effect of transient and permanent permeability transition pore opening on NAD(P)H localization in intact cells. *J Biol Chem* 284(22):15117–15125.
30. Li D, Zheng W, Qu JY (2009) Two-photon autofluorescence microscopy of multicolor excitation. *Opt Lett* 34(2):202–204.
31. Skala MC, et al. (2007) In vivo multiphoton microscopy of NADH and FAD redox states, fluorescence lifetimes, and cellular morphology in precancerous epithelia. *Proc Natl Acad Sci USA* 104(49):19494–19499.
32. Zhang SL, et al. (2006) Genome-wide RNAi screen of Ca^{2+} influx identifies genes that regulate Ca^{2+} release-activated Ca^{2+} channel activity. *Proc Natl Acad Sci USA* 103(24): 9357–9362.
33. Balaban RS (2009) The role of Ca^{2+} signaling in the coordination of mitochondrial ATP production with cardiac work. *Biochim Biophys Acta* 1787(11):1334–1341.
34. Hung YP, Albeck JG, Tantama M, Yellen G (2011) Imaging cytosolic NADH-NAD^+ redox state with a genetically encoded fluorescent biosensor. *Cell Metab* 14(4):545–554.
35. Abdelwahid E, et al. (2007) Mitochondrial disruption in *Drosophila* apoptosis. *Dev Cell* 12(5):793–806.
36. Dorstyn L, Mills K, Lazebnik Y, Kumar S (2004) The two cytochrome *c* species, DC3 and DC4, are not required for caspase activation and apoptosis in *Drosophila* cells. *J Cell Biol* 167(3):405–410.
37. Kushnareva YE, Sokolove PM (2000) Prooxidants open both the mitochondrial permeability transition pore and a low-conductance channel in the inner mitochondrial membrane. *Arch Biochem Biophys* 376(2):377–388.
38. Wei AC, Liu T, Winslow RL, O'Rourke B (2012) Dynamics of matrix-free Ca^{2+} in cardiac mitochondria: Two components of Ca^{2+} uptake and role of phosphate buffering. *J Gen Physiol* 139(6):465–478.
39. Chalmers S, Nicholls DG (2003) The relationship between free and total calcium concentrations in the matrix of liver and brain mitochondria. *J Biol Chem* 278(21): 19062–19070.
40. Lee Y, et al. (2015) Structure and function of the N-terminal domain of the human mitochondrial calcium uniporter. *EMBO Rep* 16(10):1318–1333.
41. Pacher P, Hajnóczky G (2001) Propagation of the apoptotic signal by mitochondrial waves. *EMBO J* 20(15):4107–4121.
42. Vais H, et al. (2015) MCUR1, CCDC90A, is a regulator of the mitochondrial calcium uniporter. *Cell Metab* 22(4):533–535.
43. Csordás G, et al. (2013) MICU1 controls both the threshold and cooperative activation of the mitochondrial Ca^{2+} uniporter. *Cell Metab* 17(6):976–987.
44. Kamer KJ, Mootha VK (2014) MICU1 and MICU2 play nonredundant roles in the regulation of the mitochondrial calcium uniporter. *EMBO Rep* 15(3):299–307.
45. Mallilankaraman K, et al. (2012) MICU1 is an essential gatekeeper for MCU-mediated mitochondrial Ca^{2+} uptake that regulates cell survival. *Cell* 151(3):630–644.
46. Patron M, et al. (2014) MICU1 and MICU2 finely tune the mitochondrial Ca2+ uniporter by exerting opposite effects on MCU activity. *Mol Cell* 53(5):726–737.
47. Perocchi F, et al. (2010) MICU1 encodes a mitochondrial EF hand protein required for Ca^{2+} uptake. *Nature* 467(7313):291–296.
48. Chung JJ, et al. (2014) Structurally distinct Ca^{2+} signaling domains of sperm flagella orchestrate tyrosine phosphorylation and motility. *Cell* 157(4):808–822.
49. Tantama M, Hung YP, Yellen G (2011) Imaging intracellular pH in live cells with a genetically encoded red fluorescent protein sensor. *J Am Chem Soc* 133(26): 10034–10037.
50. Grynkiewicz G, Poenie M, Tsien RY (1985) A new generation of Ca^{2+} indicators with greatly improved fluorescence properties. *J Biol Chem* 260(6):3440–3450.
51. Stotz SC, Clapham DE (2012) Anion-sensitive fluorophore identifies the Drosophila swell-activated chloride channel in a genome-wide RNA interference screen. *PloS One* 7(10):e46865.
52. Fedorenko A, Lishko PV, Kirichok Y (2012) Mechanism of fatty-acid-dependent UCP1 uncoupling in brown fat mitochondria. *Cell* 151(2):400–413.

Downloaded at Palestinian Territory, occupied on December 14, 2021

www.manaraa.com